# An Advanced Non-Interrupted Phase Synchronization Scheme with Internal Calibration for LuTan-1

Da Liang[a,b], Kaiyu Liu[a], Heng Zhang[a], Dacheng Liu[a], and Robert Wang[a]
[a]Aerospace Information Research Institute, Chinese Academy of Sciences, Beijing, China
[b]University of Chinese Academy of Sciences, Beijing, China

## Abstract

Phase synchronization is one of the key issues that must be addressed in the bistatic synthetic aperture radar (BiSAR) system. LuTan-1 is an innovative L-band spaceborne BiSAR mission of China. An advanced synchronization scheme is used in the LuTan-1 system. The synchronization pulses are exchanged immediately after the ending time of the radar echo receiving window and before the starting time of the next pulse repetition interval. Therefore, it can not interrupt the normal SAR data acquisition, further improving synchronization frequency and avoiding the data missing effect. In order to accurately monitor system malfunctions and compensate for the phase synchronization errors introduced by hardware system, an innovative internal calibration strategy is designed and employed in the LuTan-1 mission. The test data acquired from the ground validation system of LuTan-1 are used to demonstrate the feasibility of the proposed scheme. The results validate the effectiveness of the proposed scheme and prove the promise for its future application in LuTan-1.

## 1 Introduction

The bistatic synthetic aperture radar (BiSAR) systems have attracted increasing attention in the last few years [1], [2]. Because BiSAR systems operate with distinct transmitter and receiver mounted on separated platforms, they can increase the capability, flexibility and performance of SAR systems [3]. LuTan-1 (as shown in **Figure 1**) is an innovative spaceborne BiSAR mission based on the use of two radar satellites operation in L-band to generate the global digital terrain models in the single-pass interferometry mode. Both satellites in this mission have the capacity to transmit and receive electromagnetic signals.

Synchronization is one of the most challenging problems in the BiSAR system [4], [5], [6]. In the last few years, many phase synchronization methods have been proposed. The continuous duplex synchronization scheme was proposed in [7]. In this method, both satellites continuously transmit the synchronization signal during the data acquisition. In [4], the pulsed duplex synchronization and pulsed alternate synchronization schemes were proposed. The TanDEM-X uses the pulsed alternate synchronization and its performance prediction was evaluated in [8]. However, the normal SAR data acquisition for TanDEM-X is periodically interrupted, leading to a periodic data loss. Thus recovery methods, such as PG algorithm and AR-Burg algorithm, are used to reconstruct the missing raw data, increasing the complexity of data processing [9]. The non-interrupted phase synchronization is proposed for LuTan-1 [10], [11]. Unlike the phase synchronization scheme for TanDEM-X, it exchanges the synchronization pulses immediately after the ending time of the radar echo receiving windows and before the starting time of next pulse repetition interval (PRI). Therefore, it can not interrupt the normal SAR data acquisition, further improving synchronization frequency and avoiding the data missing effect.

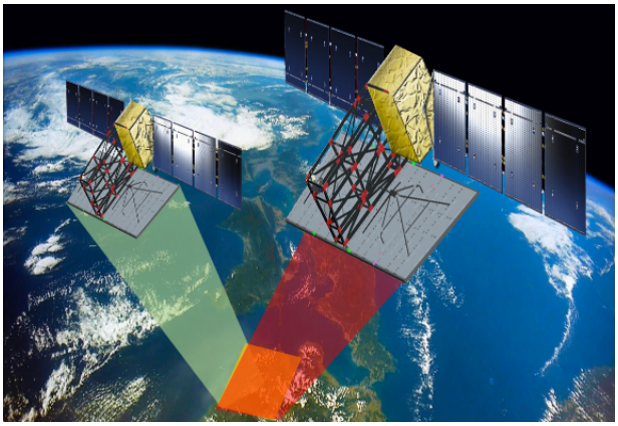

**Figure 1** Artist's view of LuTan-1 satellites.

Compared with the traditional monostatic SAR system, the application of high-accuracy synchronization link increases the complexity of the BiSAR system. Therefore, the internal calibration of the system is essential to ensure system stability and signal quality. In order to accurately monitor the system malfunctions and compensate for the phase errors introduced by hardware system, an innovative internal calibration strategy is designed and employed in the LuTan-1 mission.

This paper is organized as follows. The LuTan-1 system design is introduced in Section 2. The non-interrupted synchronization scheme is described in Section 3. In Section 4, the internal calibration scheme of LuTan-1 is introduced. Section 5 gives the system test results of LuTan-1 ground validation system. Section 6 concludes the paper.

## 2 LuTan-1 system design

LuTan-1 is an innovative spaceborne bistatic observation mission which is the first Chinese spaceborne bistatic SAR mission for civil applications, and contains two advanced L-band high-resolution wide-swath full-polarimetric SAR systems with flexible formation flying. It will be launched in beginning of 2021.

**Table 1** LuTan-1 system parameters

| Parameter | Value |
|---|---|
| Orbit Height | 607 km |
| Carrier Frequency | 1.26 GHz |
| SAR Payload Mass | 1250 kg |
| Peak Power | 16000 W |
| Antenna Length | 9.8 m |
| Antenna Width | 3.4 m |
| Polarization | single/quad/compact |
| Bandwidth | 80 MHz |
| Baseline | 0.5 km∼8 km |
| PRF | 1400 Hz∼4500 Hz |

The main system parameters can be seen in **Table 1**. The carrier frequency is 1.26 GHz. The active phased array antenna has an overall aperture size of 9.8 m×3.4 m and its peak power is 16000W. The LuTan-1 system can be operated in Stripmap and ScanSAR modes with full polarization capability. In the standard single-pass interferometry Stripmap mode of LuTan-1 mission, the swath coverage is 50 km × 50 km and the incidence angle varies from 20° to 46°.

The primary objectives of LuTan-1 mission are achieving a global digital terrain model with high accuracy, and systematically observing the deformation of the Earth's surface with millimeter accuracy for earthquake research and risk analysis. Beside this, the single-pass polarimetric SAR interferometry will be performed to measure the 3-D forest structure and biomass. The unique data set acquired by LuTan-1 is of great promise for extensive and new scientific applications.

## 3 Synchronization concept

In the BiSAR system, the two oscillators have some deviation, that will severely degrade the quality of the SAR image [5]. To achieve phase synchronization for BiSAR, a phase synchronization link is needed to realize phase synchronization prior to imaging processing by the bidirectional pair transmission between the primary satellite and the slave satellite. In this section, an advanced non-interrupted phase synchronization scheme for LuTan-1 is analysed. A general mathematical model for the synchronization scheme is also described in detail.

### 3.1 Synchronization link in LuTan-1

The timing diagram of the synchronization pulse exchange in the case of primary satellite transmits radar signal is shown in **Figure 2** (the timing diagram of the synchronization pulse exchange in the case of slave satellite transmits radar signal is similar). There are two free durations for synchronization. The first free duration is free duration between the time of the end of the radar signal transmission and the starting time of radar echo receiving windows, and correspondingly, the second free duration is the free duration between the time of the end of radar echo receiving window and the starting time of the next PRI. In the proposed synchronization scheme, the phase synchronization signal is exchanged in the second free duration. This prevents the interruptions of the normal SAR operation of LuTan-1. Therefore, there is no need to consider the problem of missing SAR data.

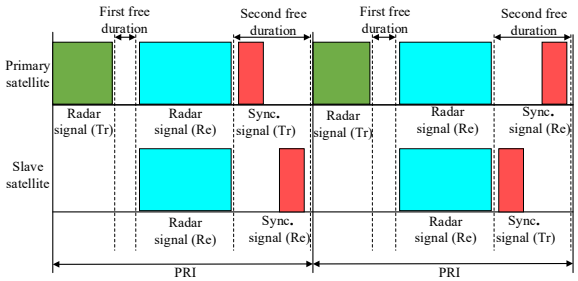


**Figure 2** Timing diagram of synchronization pulse exchange in the case of primary satellite transmits radar signal.

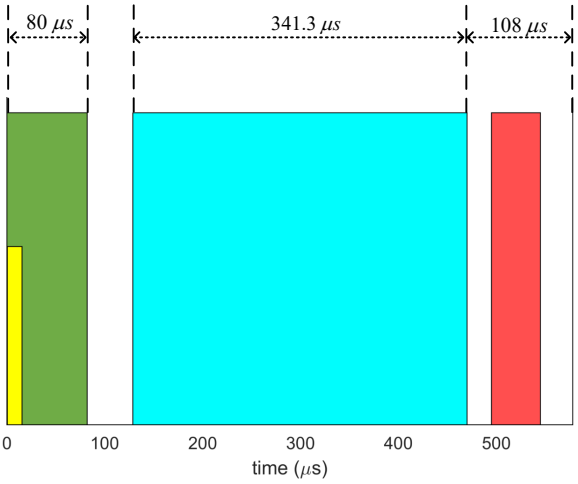


**Figure 3** Timing diagram of a typical beam in LuTan-1 mission. Yellow rectangle represents nadir echo.

**Table 2** One typical beam of LuTan-1 Stripmap mode

| Parameter | Value |
|---|---|
| Incidence Angle | 42.90° ∼ 46.08° |
| Radar Pulse Width | 80 $\mu$s |
| Echo Receiving Window Width | 341.3 $\mu$s |
| Synchronization Pulse Width | 10 $\mu$s |
| PRF | 1730 Hz |

One typical beam of LuTan-1 Stripmap mode is shown in

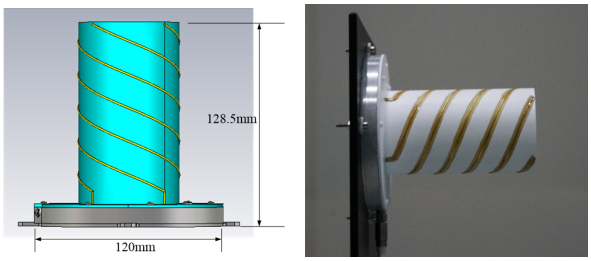


(a) (b)

**Figure 4** Quadrifilar helix antenna used for synchronization. (a) Antenna size. (b) Photograph of a quadrifilar helix antenna.

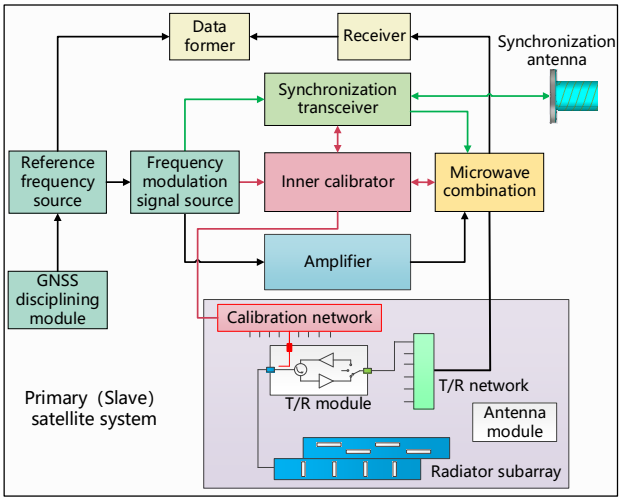


**Figure 5** The structure block diagram of the LuTan-1 system.

**Table 2**. The pulse repetition frequency (PRF) is 1730 Hz. Correspondingly, the PRI is 578 $\mu$s. The timing diagram of this beam is shown in **Figure 3**. The second free duration is 108 $\mu$s, which can be used for synchronization. The baseline of two satellites is less than 10 km, so the transmission time is less than 34 $\mu$s. The synchronization pulse width is 10 $\mu$s. Therefore, the second free duration is enough for synchronization signal transmission and reception.

The chirp signal with the same carrier frequency as the transmitted radar signal is used in the synchronization link, thereby reducing the complexity of system design. After pulse compression, a phase value with high SNR will be extracted in the peak position. The maximum value of synchronization frequency can be set to the half of PRF. In order to achieve omnidirectional coverage during an orbital period, both primary and slave satellites are equipped with four circular polarized L-band quadrifilar helix antennas (see **Figure 4**), which are used for transmitting and receiving the synchronization signal.

### 3.2 Synchronization system model

Suppose the nominal frequency is $f_0$. The frequency of oscillator $i$ at time $t$ is $f_i(t) = f_0 + \Delta f_i(t)$, where $i \in \{1, 2\}$, $\Delta f_i(t)$ denotes the frequency offset at time $t$. The demodulated phase $\varphi_{ji}$ is available at satellite $j$ for a signal transmitted by satellite $i$. The phase differences $\varphi_{12}$ and $\varphi_{21}$ are used to obtain the compensation phase $\varphi_c$. The $\varphi_c$ can be expressed as [4]

$$\begin{aligned}\varphi_c &= \frac{1}{2}(\varphi_{21} - \varphi_{12}) \\ &\approx 2\pi\Delta f(t)t + \pi\Delta f(t)(\tau + \tau_{sys}) - \pi f_D \tau_{sys} + \varphi_{oth}\end{aligned} \tag{1}$$

where $\Delta f(t) = \Delta f_1(t) - \Delta f_2(t)$ is the frequency offset between two oscillators, and $\tau$ denotes the synchronization pulse travel time between the two satellites. The transmit instance of satellite 2 is delayed by $\tau_{sys}$ with respect to satellite 1, and $f_D$ is the Doppler frequency due to the relative velocity between the two satellites. $\varphi_{oth}$ is the other phase errors which include the initial phase difference between two oscillators, oscillator noise phase error, antenna phase error and hardware system phase error.

## 4 Internal calibration system for phase synchronization

From the synchronization phase compensation formula in Section 3, it can be seen that the phase error introduced by hardware system will effect the performance of the synchronization scheme. In order to accurately monitor system malfunctions and compensate for the phase synchronization errors introduced by hardware system, an innovative internal calibration strategy is designed and employed in the LuTan-1 mission.

### 4.1 Ground validation system for LuTan-1

The diagram of ground validation system for LuTan-1 is illustrated in **Figure 5**. The system consists of signal generation, transmit-receive and calibration units. The signal generation unit consists of the Global Navigation Satellite System (GNSS) disciplining module, reference frequency source and frequency modulation signal and is arranged to generated the linear frequency modulation (LFM) signal for imaging or synchronization. The GNSS disciplining module employs disciplined rubidium clock to provide a time frequency signal for reference frequency source module, and the multiple working frequency signals that are used to generate the corresponding radar signal by the frequency modulation signal source are generated by the reference frequency source. The transmit-receive unit, which consists of microwave combination, synchronization transceiver, receiver and data former, controls the transmitting and receiving of the signal.

### 4.2 Internal calibration

The five phase internal calibration loops in the primary and slave satellites are briefly presented in **Figure 6**, which corresponds to the hardware system in **Figure 5**. For the sake of simplicity, some components are integrated according to their functions. In here, $LFM$ denotes the signal generation unit and $TX$ depicts the transmitting unit (amplifier and microwave combination). The antenna receiving

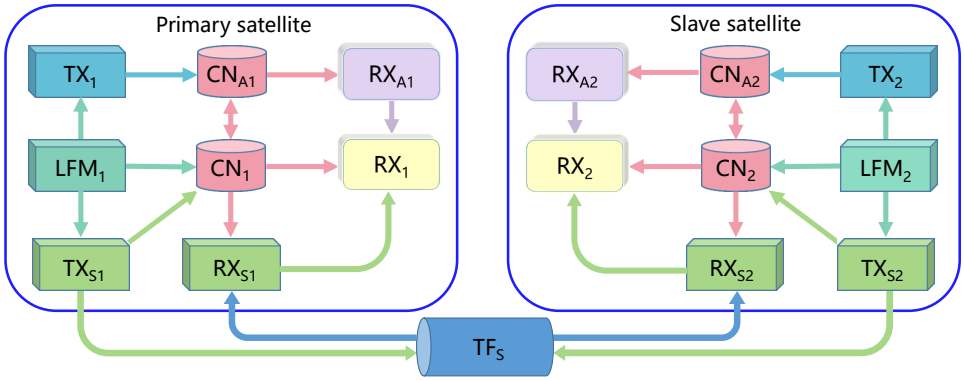


**Figure 6** The internal calibration loops and synchronization transmission in the LuTan-1 system.

channel is represents by $RX_A$. $RX$, which consists of microwave combination, receiver and data former, represents the part of the receiving unit except the antenna receiving channel. $CN$ and $CN_A$ refer to the internal calibration subassembly and antenna calibration network, respectively. $TX_S$ and $RX_S$ represent transmitting chain and receiving chain of synchronization transceiver, respectively. The internal calibration strategy is based on five calibration loops: chirp transmitting calibration loop $TX_{cal}$, chirp receiving calibration loop $RX_{cal}$, chirp reference calibration loop $CE_{cal}$, synchronization transmitting calibration loop $ST_{cal}$, and synchronization receiving calibration loop $SR_{cal}$. The transfer functions of the five calibration loops can be written as follows

$$TX^i_{cal} = LFM_i \cdot TX_i \cdot CN_{Ai} \cdot CN_i \cdot RX_i \tag{2a}$$
$$RX^i_{cal} = LFM_i \cdot CN_i \cdot CN_{Ai} \cdot RX_{Ai} \cdot RX_i \tag{2b}$$
$$CE^i_{cal} = LFM_i \cdot CN_i \cdot RX_i \tag{2c}$$
$$ST^i_{cal} = LFM_i \cdot TX_{Si} \cdot CN_i \cdot RX_i \tag{2d}$$
$$SR^i_{cal} = LFM_i \cdot CN_i \cdot RX_{Si} \cdot RX_i. \tag{2e}$$

In BiSAR mode of LuTan-1, one satellite transmits the radar signal and both satellites receive the echoes from the ground. However, the paths of the signal through the instrument in two satellites are different. The transfer function $H_C$ that compensates the influence of the bistatic signal path can be written as

$$H_C = \frac{RX_{A2} \cdot RX_2}{RX_{A1} \cdot RX_1}. \tag{3}$$

The transfer function of the synchronization link where the primary satellite transmits the signal and the slave satellite receives the signal can be written as

$$HS_{21} = LFM_1 \cdot TX_{S1} \cdot TF_S \cdot RX_{S2} \cdot RX_2 \tag{4}$$

where $TF_S$ is the transfer function of synchronization signal in space transmission. Similarity, the transfer function of the synchronization link where the slave satellite transmits and the primary satellite receives is

$$HS_{12} = LFM_2 \cdot TX_{S2} \cdot TF_S \cdot RX_{S1} \cdot RX_1. \tag{5}$$

Combining Eq. (2d), (2e), (4) and (5), the following equation can be obtained

$$\sqrt{\frac{HS_{21}}{HS_{12}}} \cdot \sqrt{\frac{SR^1_{cal}}{SR^2_{cal}}} \cdot \sqrt{\frac{ST^2_{cal}}{ST^1_{cal}}} = \sqrt{\frac{LFM_1 \cdot RX_2}{LFM_2 \cdot RX_1}}. \tag{6}$$

Combining Eq. (2b) and (2c), we have

$$\frac{RX^2_{cal}}{RX^1_{cal}} \cdot \frac{\sqrt{CE^1_{cal}}}{\sqrt{CE^2_{cal}}} = \frac{\sqrt{LFM_2 \cdot CN_2 \cdot RX_2}}{\sqrt{LFM_1 \cdot CN_1 \cdot RX_1}} \cdot \frac{CN_{A2} \cdot RX_{A2}}{CN_{A1} \cdot RX_{A1}}. \tag{7}$$

Therefore, combining Eq. (6) and (7), the compensation formula of the entire BiSAR path can be expressed as

$$H_C = K \cdot \sqrt{\frac{HS_{21}}{HS_{12}}} \cdot \sqrt{\frac{SR^1_{cal}}{SR^2_{cal}}} \cdot \sqrt{\frac{ST^2_{cal}}{ST^1_{cal}}} \cdot \frac{RX^2_{cal}}{RX^1_{cal}} \cdot \frac{\sqrt{CE^1_{cal}}}{\sqrt{CE^2_{cal}}} \tag{8}$$

where $K = CN_{A1} \cdot \sqrt{CN_1}/(CN_{A2} \cdot \sqrt{CN_2})$ is related to the transfer function of the internal calibration subassembly and the antenna calibration network. The characteristics of the calibration subassembly may change due to aging effect and temperature variation. However, the variation within an acquisition is negligible. The phase offset of the calibration subassembly is almost constant. Therefore, $K$ can be regarded as a constant and is ignorable in the analysis. As a result, the accurate compensation phase $\varphi_{ac}$ for the entire path in the LuTan-1 system can be written as

$$\varphi_{ac} = \frac{1}{2}(\varphi_{21} - \varphi_{12}) + \frac{1}{2}\left(\varphi_{SR^1_{cal}} - \varphi_{SR^2_{cal}}\right) - \frac{1}{2}\left(\varphi_{ST^1_{cal}} - \varphi_{ST^2_{cal}}\right) - \left(\varphi_{RX^1_{cal}} - \varphi_{RX^2_{cal}}\right) + \frac{1}{2}\left(\varphi_{CE^1_{cal}} - \varphi_{CE^2_{cal}}\right) \tag{9}$$

where $\varphi_{RX^i_{cal}}, \varphi_{CE^i_{cal}}, \varphi_{ST^i_{cal}}$ and $\varphi_{SR^i_{cal}}$ are the phases of $RX^i_{cal}, CE^i_{cal}, ST^i_{cal}$ and $SR^i_{cal}$ correspondingly. The first term in Eq. (9) is the same as Eq. (1), which is used to compensate frequency offset caused by oscillator deviation. Other items in Eq. (9), which can be regarded as phase drift in internal calibration, are used to correct the phase errors introduced by hardware system.

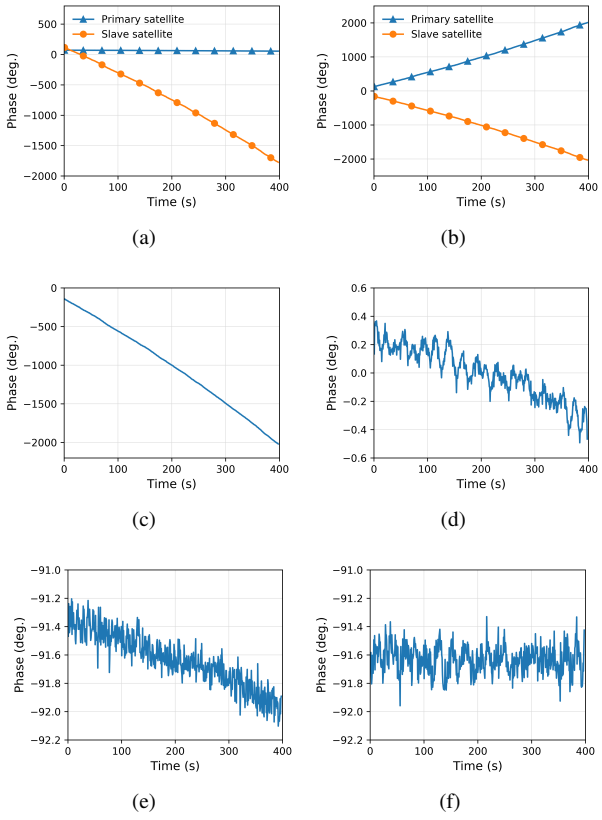


**Figure 7** (a) Imaging signal phase. (b) Synchronization signal phase, primary satellite denotes $\varphi_{12}$ and slave satellite denotes $\varphi_{21}$. (c) Phase difference $(\varphi_{21} - \varphi_{12})/2$ of synchronization signals. (d) Phase drift in internal calibration. (e) Residual phase without internal calibration. (f) Residual phase with internal calibration.

# 5 Performance evaluation

In the experiment, the imaging signal phase of the two satellites is observed in **Figure 7** (a). Since the primary satellite operates spontaneously, its imaging signal phase is almost constant over time, while the image signal phase of slave satellite changes over time. For the imaging signals of slave satellites, the phase history changes with time due to the frequency difference between two oscillators. During the working period, the phase difference of imaging signals between the two satellites is as high as several thousand degrees. **Figure 7** (b) depicts the phase history of the corresponding synchronization signals during radar imaging. **Figure 7** (c) depicts phase difference $(\varphi_{21} - \varphi_{12})/2$ of synchronization signals in **Figure 7** (b). The phase history of the internal calibration pulses during radar imaging is shown in **Figure 7** (d). The residual phase after compensation without internal calibration can be seen in **Figure 7** (e) and the STD of the residual phase is $0.214$ degrees. Applying the system internal calibration, the instrument drift can be accurately determined and calibrated. The residual phase after compensation by Eq. (9) is displayed in **Figure 7** (f) and the STD of the residual phase is $0.123$ degrees, which verifies that the phase synchronization scheme with internal calibration has high accuracy.

# 6 Conclusion

Phase synchronization is one of the key issues that must be addressed in the BiSAR system. LuTan-1 is an innovative L-band spaceborne BiSAR mission of China. An advanced non-interrupted phase synchronization scheme with internal calibration is used in the LuTan-1 mission. The calibration loops cover all the hardware components that the imaging and synchronization signals pass through, therefore, the calibration strategy can monitor the working status of hardware in different working environments and ensure system stability. The test results validate the effectiveness of the proposed method and prove the promise for the future application in LuTan-1.

# 7 Literature

[1] G. Krieger and F. D. Zan, “Relativistic effects in bistatic synthetic aperture radar,” IEEE Trans. Geosci. Remote Sens., vol. 52, no. 2, pp. 1480–1488, Feb. 2013.

[2] H. Zhang et al., “Spaceborne/Stationary bistatic SAR imaging with TerraSAR-X as an illuminator in staring-spotlight mode,” IEEE Trans. Geosci. Remote Sens., vol. 54, no. 9, pp. 5203–5216, Sep. 2016.

[3] G. Krieger et al., “TanDEM-X: A radar interferometer with two formation-flying satellites,” Acta Astronautica, vol. 89, pp. 83–98, 2013.

[4] M. Younis, R. Metzig, and G. Krieger, “Performance prediction of a phase synchronization link for bistatic SAR,” IEEE Geosci. Remote Sens. Lett., vol. 3, no. 3, pp. 429–433, Jul. 2006.

[5] G. Krieger and M. Younis, “Impact of oscillator noise in bistatic and multistatic SAR,” IEEE Geosci. Remote Sens. Lett., vol. 3, no. 3, pp. 424–428, Jul. 2006.

[6] Weib M, “Synchronisation of bistatic radar systems,” in IGARSS 2004. Proceedings, 2004, 3: pp. 1750-1753.

[7] M. Eineder, “Ocillator clock drift compensation in bistatic interferometric SAR,” in IGARSS 2003. Proceedings, 2003, 3: pp. 1449–1451.

[8] H. Breit et al., “Bistatic synchronization and processing of TanDEM-X data,” in IGARSS 2011. Proceedings, 2011, pp. 2424-2427.

[9] M. Pinheiro et al., “Reconstruction of coherent pairs of synthetic aperture radar data acquired in interrupted mode,” IEEE Trans. Geosci. Remote Sens., vol. 53, no. 4, pp. 1876–1893, Apr. 2015.

[10] D. Liang et al., "An advanced non-interrupted synchronization scheme for bistatic synthetic aperture radar," in IGARSS 2019. Proceedings, 2019, pp. 1116-1119.

[11] D. Liang et al., "A high-accuracy synchronization phase-compensation method based on Kalman filter for bistatic synthetic aperture radar," in IEEE Geosci. Remote Sens. Lett..